

## Dimensional transition in Darcy-Rayleigh-Taylor mixing

M. Borgnino <sup>1,2</sup>, G. Boffetta,<sup>2</sup> and S. Musacchio<sup>2</sup>

<sup>1</sup>*Dipartimento di Ingegneria dell'Ambiente, del Territorio e delle Infrastrutture, Politecnico di Torino, Torino, Italy*

<sup>2</sup>*Dipartimento di Fisica and INFN, Università di Torino, 10125 Torino, Italy*



(Received 24 February 2021; accepted 9 July 2021; published 23 July 2021)

When a fluid is confined in a thin layer, it undergoes a dramatic change in its dynamical and/or statistical properties, which occurs when the confining scale is of the order of some characteristic scale of the flow. Here we study this *dimensional transition* in the framework of Rayleigh-Taylor mixing in porous media. By means of extensive direct numerical simulations of the Darcy-Rayleigh-Taylor model, we demonstrate the existence of a transition from three-dimensional (3D) to 2D phenomenology when the horizontal width of the convective structures becomes larger than the confining scale. At variance with the case of turbulent flows, in which the transition is continuous and a coexistence of the 2D and 3D regimes is observed, the transition in porous media is sharp. We investigate the effects of the transition on the evolution of the mixing process and on the fluctuations of the density field. In the 2D regime, we observe a speedup in the growth rate of the mixing layer with an increase of the inhomogeneities of the density field.

DOI: [10.1103/PhysRevFluids.6.074501](https://doi.org/10.1103/PhysRevFluids.6.074501)

### I. INTRODUCTION

The Darcy-Rayleigh-Taylor (DRT) flow is a prototype of convective mixing in porous media. In analogy with the classical Rayleigh-Taylor (RT) setup, when a layer of heavier fluid is placed on top of a layer of fluid with lower density in presence of a relative acceleration, the interface between the two layers becomes unstable [1]. The evolution of the interface leads to the development of a mixing layer between the two fluids.

When this process occurs in the bulk of a porous medium, the dynamics of the buoyancy-driven flow is properly described by the Darcy's law, instead of the Navier-Stokes equations. As a consequence, the properties of convective mixing in porous media are different from those of the turbulent convective mixing observed in the classical RT case. While the latter has been extensively investigated since the last century (see Refs. [2,3] for recent reviews), convective mixing in porous media is less studied. Gravity driven flow in porous media are important in many applications, in particular in CO<sub>2</sub> sequestration in saline aquifers [4–7], and this motivated recent numerical and experimental studies of the DRT instability. Most of these studies have been performed in 2D [8–11] and a few in 3D [12,13].

The dimensionality of the flow plays a crucial role in its dynamics and statistical properties and the transition between 3D and 2D regimes in turbulent flows has been object of extensive studies in the past decade (see Ref. [14] for a recent review). In the case of turbulent flows sustained by an external forcing, the transition occurs when the confined dimension of the layer becomes smaller than the forcing correlation scale [15–17]. This transition is smooth and for intermediate confinement one observes the coexistence of a direct and an inverse energy cascade. In the case of RT turbulence, the transition occurs dynamically when the width of the turbulent mixing region becomes larger than the confined dimension of the fluid layer [18]. In this case the transition changes

not only the direction but also the statistics of the cascade, from Kolmogorov-Obukhov scaling in 3D [19] to Bolgiano-Obukhov scaling in 2D [20,21]. Also in this case it is possible to observe both scaling laws at intermediate confinement [18]. In the DRT case the dimensionality changes quantitatively the evolution of the mixing layer. In particular, it has been observed a faster growth of the mixing layer in 2D simulations with respect to 3D simulations at the same Péclet number [13].

In this work we investigate the nature of the dimensional transition in mixing convection in a porous medium confined in a vertical layer. To this aim, we numerically study the Darcy-Rayleigh-Taylor flow in a domain in which the vertical size  $L_z$  is much larger than the horizontal sizes  $L_x$  and  $L_y$  and the latter (the confined direction) varies in the range  $0 < L_y \leq L_x$ . By extensive direct numerical simulation of the DRT model, we find that the evolution of the system with different  $L_y$  can be grouped in two classes characterized by either 2D or 3D dynamics with a sharp transition. The discriminant between the two classes is whether the scale  $L_y$  is smaller or larger than the typical horizontal scale of the convective structures which develop in the mixing layer.

## II. DARCY-RAYLEIGH-TAYLOR SYSTEM

We consider the Darcy's equation to describe the motion of a single-phase fluid in a porous media [22]. In the Boussinesq approximation [23] the equations for the density field  $\rho$  and the incompressible velocity field  $\mathbf{u}$  are as follows:

$$\partial_t \rho + \mathbf{u} \cdot \nabla \rho = D \nabla^2 \rho, \quad (1)$$

$$\mathbf{u} = \frac{\kappa}{\mu \phi} (-\nabla p + \rho \mathbf{g}), \quad \nabla \cdot \mathbf{u} = 0, \quad (2)$$

where  $\mathbf{g} = (0, 0, -g)$  is the gravitational acceleration,  $D$  is the diffusivity coefficient,  $\phi$  is the porosity of the medium and  $\kappa$  is the isotropic permeability. The viscosity  $\mu$  is assumed to be constant. The pressure  $p$  is given by the Poisson equation  $\nabla^2 p = \rho g \kappa / (\mu \phi)$  and the Darcy flow rate is  $\mathbf{q} = \phi \mathbf{u}$ .

By imposing an initial unstable step density profile  $\rho = \rho_0 + \text{sgn}(z) \Delta \rho / 2$  in the vertical direction, where  $\Delta \rho$  is the density jump at the interface in  $z = 0$ , we obtain a Rayleigh-Taylor configuration with Atwood number  $A = \Delta \rho / 2 \rho_0$  (as in Ref. [13]). The value of the mean density  $\rho_0$  does not affect the dynamics since the term  $\rho_0 \mathbf{g}$  in Eq. (2) can be absorbed in the hydrostatic pressure. Therefore, in the following, we set  $\rho_0 = 0$  without loss of generality. The density jump defines the characteristic velocity of the system  $w_0 = \frac{kg}{\mu \phi} \Delta \rho$  which enters in the dimensionless Péclet number  $\text{Pe} = L_x w_0 / D$ . We remark that the model (1-2) is incompressible by definition, independently on the value of  $A$ , and this limits the physical applicability of the DRT model to small Atwood number. Moreover, the Darcy equation (2) is valid for a Reynolds number based on the pore diameter  $d$  smaller than unit [24]. Since the permeability is proportional to  $d^2$ , Using  $w_0$  as the typical velocity one can write  $\text{Re} \simeq d^3 g A / (v^2 \Phi) < 1$  which gives a condition for the maximum pore size.

In order to investigate the transition from the 2D to the 3D regime, we consider the Darcy-Rayleigh-Taylor flow in a domain of size  $L_x, L_y, L_z$  with  $L_z \gg L_x \geq L_y$  at varying transverse dimension  $L_y$ . Linear stability analysis shows that the most unstable mode in DRT system has a wavelength  $L_D = \frac{4\pi}{\sqrt{5-2}} \frac{D}{w_0}$  [8,25,26]. When the transverse scale  $L_y$  is smaller than  $L_D$ , instabilities cannot develop in the  $y$  direction and the dynamics is expected to be two dimensional. Three-dimensional flow can only develop when  $L_y \gg L_D$ . We therefore introduce the dimensionless *confinement number*  $R \equiv L_y / L_D$  which we will use to parametrize the transition from 2D to 3D regime. We notice that also the Péclet number can be interpreted as a confining number in the  $x$  direction because it can be rewritten as  $\text{Pe} = L_x w_0 / D = \frac{L_x}{L_D} \frac{4\pi}{\sqrt{5-2}}$ . Therefore it is not expected to influence the dimensional transition, provided that it is sufficiently large ( $\text{Pe} \gg 1$ ).

TABLE I. Summary of the geometry of the simulations.  $N_y$  is number of grid points in the  $y$  direction,  $R = L_y/L_D$ , and  $M$  is the number of realization per each width  $L_y$ .

$N_y$	1	2	4	8	16	24	32	64	128	256	512	2048
$L_y$	$\pi/1024$	$\pi/512$	$\pi/256$	$\pi/128$	$\pi/64$	$3\pi/128$	$\pi/32$	$\pi/16$	$\pi/8$	$\pi/4$	$\pi/2$	$2\pi$
$R$	0.29	0.58	1.15	2.31	4.61	6.92	9.22	18.4	36.9	73.8	148	590
$M$	10	15	15	20	15	15	10	10	5	3	1	1

### III. NUMERICAL SIMULATIONS

We performed a large series of numerical simulations of the Darcy-Boussinesq equations (1) and (2) in a triply periodic domain with size  $L_x = 2\pi$ ,  $0 < L_y \leq L_x$ , and  $L_z = 4L_x$ , at fixed Péclet number  $Pe = \pi \times 10^4$ . The equations are discretized on a uniform grid at resolution  $N_x = 2048$ ,  $N_y = N_x(L_y/L_x)$ , and  $N_z = 4N_x$ . The corresponding values of the confinement  $R$  are reported in Table I and vary from  $R = 0.29$  (which correspond to a 2D simulation with  $N_y = 1$ ) up to  $R = 590$  (fully 3D case with  $L_y = L_x$ ).

At initial time  $t = 0$  the density field is set to  $\rho(x, y, z, t = 0) = \text{sgn}(z)\Delta\rho/2$  for  $-L_z/2 < z < L_z/2$ . In our simulations the mean density is set to  $\langle \rho \rangle = 0$  (as discussed in Sec. II), and the density jump is  $\Delta\rho = 1$ . A small, random perturbation is added at time  $t = 0$  at the interface at  $z = 0$  to trigger the instability. In order to improve the statistical accuracy, the results for each dimension  $L_y$  have been averaged over a set of  $M$  simulations with independent realizations of the initial random perturbation (see Table I).

The simulations are performed by means of a fully parallel pseudospectral code, with 2/3 dealiasing and second-order Runge-Kutta time scheme with explicit integration of the diffusive term in (1). A zero-velocity mask is imposed at the stable density jump at  $z = \pm L_z/2$ . Further details of the numerical code and of its validation are reported in Ref. [13].

For the discussion of the results in the next section we will use three different spatial averages: the 3D average over the whole volume  $\langle \dots \rangle \equiv (1/L_x L_y L_z) \iiint \dots dx dy dz$ , the 2D average over the  $xy$  plane  $\langle \dots \rangle_{xy} \equiv (1/L_x L_y) \iint \dots dx dy$ , and the 1D average over the  $x$  direction  $\langle \dots \rangle_x \equiv (1/L_x) \int \dots dx$  (and similarly for  $y$ ). The average over the  $M$  realizations is implied for all the results presented (excluding the plots in Figs. 1 and 5).

### IV. RESULTS

The effects of the confinement in the  $y$  direction of the Darcy-Rayleigh-Taylor flow are clearly visible by comparing the density field obtained in the simulations with different confinement number  $R$ . In Fig. 1 we show the sections of the density field in the  $xz$  plane for  $R = 0.58$  ( $N_y = 2$ ),  $R = 4.61$  ( $N_y = 16$ ), and  $R = 36.9$  ( $N_y = 128$ ) (from left to right) at the same time  $t = 4.9\tau$  (we use  $\tau = L_x/w_0$  to make time dimensionless). In all the cases, we observe the development of a mixing layer characterized by thin, elongated structures (“fingers”) which penetrate symmetrically into the upper and bottom reservoirs. The length and width of the fingers are influenced by the confinement: The height of the mixing layer is reduced at increasing  $R$ , while the horizontal scale of the fingers displays a nonmonotonic dependence on  $R$ , with a maximum at intermediate  $R$ .

The dependence on  $R$  of the extension of the mixing layer is confirmed by the inspection of the mean density profiles  $\bar{\rho}(z, t)$ . They are computed by averaging the density field over the  $x$  and  $y$  directions  $\bar{\rho}(z, t) = \langle \rho(x, y, z, t) \rangle_{xy}$  with a further average over the  $M$  realizations. As shown in Fig. 2(a), at fixed time the profiles can be divided in two clusters: below a certain transverse scale  $L_y$  (corresponding to  $R \simeq 5$ ) the profiles are indistinguishable from the 2D one ( $N_y = 1$ ) while above that scale they almost coincide with that of the full 3D case ( $R = 590$ ). At fixed time, the extension of the profiles belonging to the 2D-like cluster is larger than that of the 3D one.

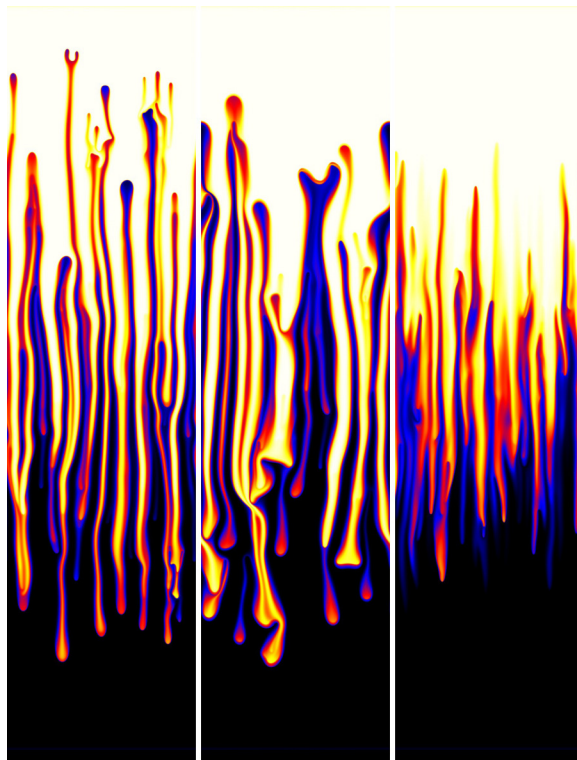


FIG. 1. Sections of the density field in the  $xz$  plane at time  $t = 4.9\tau$  for the simulations at  $R = 0.58$  (left),  $R = 4.61$  (middle), and  $R = 36.9$  (right). The colors scale ranges from the density values  $\rho = -\Delta\rho/2$  (black) to  $\rho = +\Delta\rho/2$  (white).

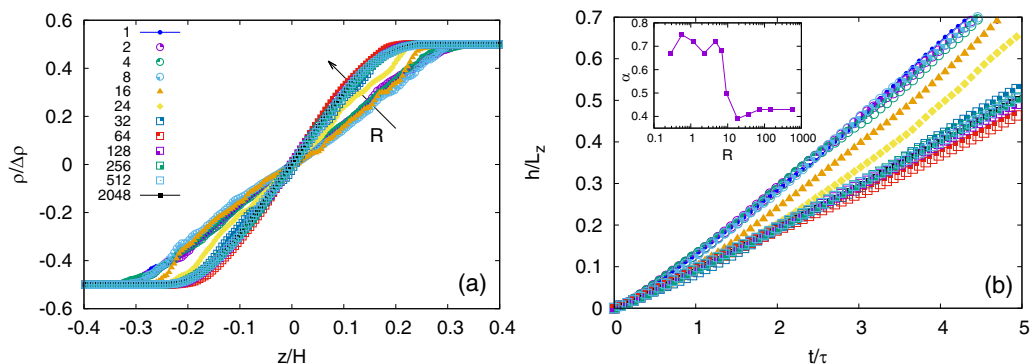


FIG. 2. (a) Mean density profiles  $\bar{\rho}(z, t)$  at time  $t = 3.5\tau$ . (b) Temporal evolution of the width  $h(t)$  of the mixing layer. Inset: Slope  $\alpha$ , obtained from a fit of  $h(t)$  with  $\alpha w_0 t$  at late times, as a function of  $R$ . Different colors and symbols represent simulations at different  $N_y$ : Blue solid line with filled circles is the two-dimensional case  $N_y = 1$  while black solid line with filled square is the three-dimensional case  $N_y = 2048$ ; circles stay for  $N_y = 2$  (violet),  $N_y = 4$  (green),  $N_y = 8$  (light blue); full triangles stay for  $N_y = 16$  (orange); full diamonds for  $N_y = 24$  (yellow); squares stay for  $N_y = 32$  (blue),  $N_y = 64$  (red),  $N_y = 128$  (violet),  $N_y = 256$  (green), and  $N_y = 512$  (light blue).

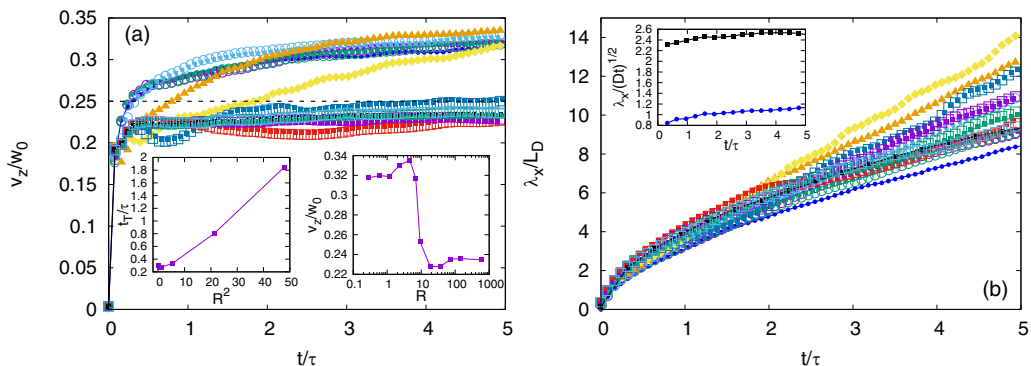


FIG. 3. (a) Time evolution of the rms vertical velocity  $v_z$  at different values of  $R$ . Inset (b): rms vertical velocity  $v_z$  at  $t = 5\tau$  versus  $L_y$  as a function of  $R$ . Inset (a): Transition time  $t_T$ , computed from the vertical velocity as the time at which  $v_z(t_T) = 0.25w_0$ , as a function of  $R^2$ . (b) Time evolution of the horizontal correlation scale  $\lambda_x(t)$  at different values of  $R$ . Inset (b):  $\lambda_x(t)$  compensated with the diffusive scaling  $(Dt)^{1/2}$ . Colors and symbols are the same of Fig. 2.

From Fig. 2 we define the width of the mixing layer as  $h(t) = z_+ - z_-$ , where  $z_{\pm}$  are the heights at which  $\bar{\rho}(z_{\pm}, t) = \pm 0.45\Delta\rho$ . Alternatives definitions of  $h(t)$  (see, e.g., Refs. [27–29]) gives qualitatively similar results. The temporal evolution of  $h(t)$  is shown in Fig. 2(b). In all cases, long-time growth of the mixing layer is compatible with a linear law  $h(t) = \alpha w_0 t$  (consequence of an asymptotic constant velocity proportional to  $w_0$  [30]) but with different coefficient  $\alpha$ . For simulations with  $R \gtrsim 10$  we have  $\alpha \simeq 0.45$ , while for small  $R \lesssim 5$  we have a faster growth with  $\alpha \simeq 0.7$ , which coincides with that of the 2D case. We remark that the values of  $\alpha$  reported here are slightly different than those measured in Ref. [13] because of the different definition of  $h(t)$ . The cases at intermediate confinement number  $R \simeq 6$  display a transition from the 3D to the 2D regime during the evolution of the dynamics: At the beginning they lie on the 3D curve, while at later time they get closer to the 2D slope.

The fastest growth of mixing layer in the quasi-two-dimensional cases is accompanied by an increase of the rms vertical velocity within the mixing layer. In Fig. 3(a) we show the temporal evolution of  $v_z(t) = (\langle u_z^2(x, y, z = 0, t) \rangle_{xy})^{1/2}$ , computed in the middle of the mixing layer at  $z = 0$ . Also in this case, the curves  $v_z(t)$  are clearly divided in two classes. In the 2D-like simulations with smaller  $L_y$ , after an initial transient the vertical velocity reaches an asymptotically constant value which is higher than the the corresponding value of the 3D-like simulations with larger  $L_y$ . The transition between the two classes is visualized by plotting the values of  $v_z(t)$  at the final time  $t = 5\tau$  as a function of the confinement number  $R$  [see inset of Fig. 3(a)]. Also in this case, close to  $R \simeq 6$ , the velocity drops down from the higher 2D plateau to the lower 3D plateau with a ratio between the two values compatible to the one observed for  $\alpha$ . From Fig. 3(a), we also note that in the two intermediate simulations with  $N_y = 16$  and  $N_y = 24$  a dimensional transition occurs during the evolution of the system. The value of  $v_z(t)$  initially lies on the 3D curve, then it grows and it reaches the 2D curve. The time at which the transition occurs is longer for the simulations with the larger  $R$ .

We argue that the transition from the 3D to the 2D regimes occurs when the transverse scale  $L_y$  is of the order of the typical horizontal width of the fingers. At the beginning of the evolution, the width of the fingers is of the order of  $L_D$ , that is the wavelength of the most unstable perturbation of the initial interface (see Sec. II). If the transverse scale  $L_y$  is smaller than or comparable with  $L_D$ , then the linear instabilities cannot develop in the  $y$  direction and the evolution of the system remains two-dimensional. Conversely, if  $L_y$  is much larger than  $L_D$ , then the 3D dynamics can develop.

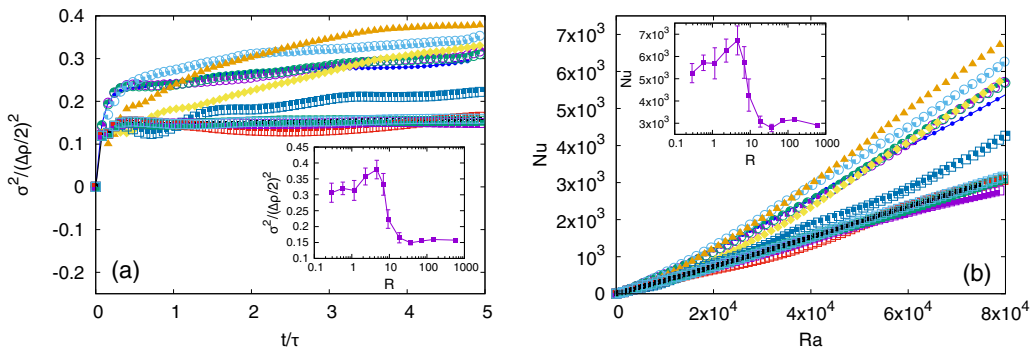


FIG. 4. (a) Time evolution of density variance  $\sigma^2 = \langle (\rho^2)_{xy} - \bar{\rho}^2 \rangle_z$ , made dimensionless with its maximum theoretical value, at different  $R$ . Inset (a): The final value of  $\sigma^2$  plotted as a function of  $R$ . (b) Nusselt number as a function of the Rayleigh number for the simulations at different values of  $R$ . Inset (b): The final value of  $Nu$  plotted as a function of  $R$ . Colors and symbols are the same of Fig. 2. Error bars represent the standard deviation over the different realizations.

This idea is indeed supported by the results shown in the insets of Fig. 2 and Fig. 3 which show a transition for  $R \simeq 6$ .

The width of fingers is expected to grow in time, because of the interplay between the processes of diffusion, merging and splitting. As a consequence, when the transverse scale  $L_y$  is larger than the initial width of the fingers, the system initially follows the 3D dynamics, and then it displays a transition to the 2D regime when the coarsening of the fingers reaches the scale  $L_y$ . In order to investigate how the width of fingers grows in time, we measure their correlation scale  $\lambda_x$  defined in terms of the autocorrelation function of the density fluctuations  $c(r, t) = \langle \rho(x+r, t)\rho(x, t) \rangle_{xy} / \langle \rho^2(x, t) \rangle_{xy}$  as the scale at which  $c(\lambda_x, t) = 1/2$  (on the plane  $z = 0$ ). The time evolution of  $\lambda_x$  is shown in Fig. 3(b). At variance with the previous results, here we cannot clearly identify two different clusters of curves belonging to the 2D and 3D regimes, nonetheless we observe a monotonic growth of the correlation scale for all the simulations. In two extreme cases with  $N_y = 1$  and  $N_y = 2048$ , which corresponds to the fully 2D and 3D simulations respectively, we identify a clear diffusive scaling  $\lambda_x \simeq (Dt)^{1/2}$  [see inset of Fig. 3(b)] in agreement with previous findings [13]. In the intermediate cases we observe some deviations from the  $t^{1/2}$  growth, but it is unclear if these deviations are transient or if they persist at longer times. Assuming that the growth of the size of fingers is responsible for the transition from 3D to 2D regimes at intermediate  $R$ , and that it follows a diffusive scaling, we obtain a simple scaling prediction for the transition time as  $t_T \propto R^2$ . This is indeed compatible with the few points  $R$  for which we observe a dynamical transition, as shown in the inset of Fig. 3(a).

It is also interesting to investigate if and how the confinement affects the mixing of the density field inside the mixing layer. To this aim we compute the density variance  $\sigma^2(t) \equiv \langle (\rho^2(x, y, z, t))_{xy} - \bar{\rho}^2(z, t) \rangle_z$  averaged over the mixing layer. For a fully mixed density field (as in the case of diffusive mixing),  $\rho$  is constant over horizontal planes, i.e.,  $\rho(x, y, z) = \bar{\rho}(z)$  and therefore  $\sigma^2 = 0$ . On the contrary, if the density field is completely unmixed (and therefore assumes values  $\pm \Delta\rho/2$  only), then the variance attains the maximum value  $\sigma^2 = \Delta\rho^2/4$ .

Figure 4(a) shows the time evolution of the variance for the simulations at different confinement  $R$ . Similarly to Fig. 3(a), also in this case 3D-like and 2D-like simulations reach different values (with some spreading of the results for the 2D-like cases). At late times, density variance reaches smaller values for the 3D simulations, indicating a better mixing with respect to the more confined simulations which have larger values as a consequence of more coherent plumes of unmixed fluid inside the mixing layer. We note that the final values of  $\sigma^2$  (computed at the last time of the simulations) display a nonmonotonic behavior as a function of  $R$  [see inset of Fig. 4(a)] They show a

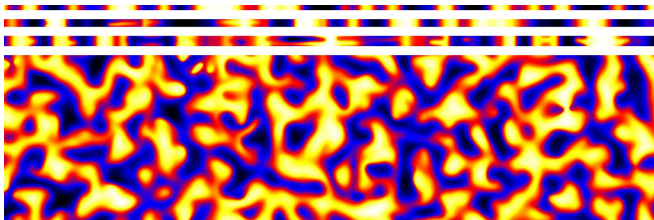


FIG. 5. Horizontal sections of the density field at  $z = 0$  and  $t = 3.5\tau$ . The four cases correspond to the simulations with  $R = 4.61$  ( $N_y = 16$ ),  $R = 6.92$  ( $N_y = 24$ ),  $R = 9.22$  ( $N_y = 32$ ), and  $R = 148$  ( $N_y = 512$ ) from top to bottom (in the plot  $x$  is along the horizontal and  $y$  along the vertical). For visualization clarity, since  $L_x \gg L_y$ , we plot only half of the section in the  $x$  direction, i.e., the region  $0 \leq x \leq L_x/2$ . The color scale ranges from the density values  $\rho = -\Delta\rho/2$  (black) to  $\rho = +\Delta\rho/2$  (white).

slight increase above the 2D value, before dropping down to the 3D value. We do not have a simple phenomenological explanation of this complex transitional behavior.

The dimensionality of the system influences also the correlations between the density fluctuations and vertical velocity field within the mixing layer. This effect can be quantified in terms of the mass-transfer Nusselt number  $Nu = \frac{\langle u_z \rho \rangle h}{D \Delta \rho}$ , which is proportional to the correlation between the fields  $u_z$  and  $\rho$ . Plotting the Nusselt number versus the Rayleigh number  $Ra = \frac{w_0 h}{D}$  allows to compare the correlation between the fields  $u_z$  and  $\rho$  in different simulations at fixed extension  $h$  of the mixing layer. The results in Fig. 4(b) show that the values of  $Nu$  at given  $Ra$  are always larger in the simulations belonging to the 2D class. The values of  $Nu$  at final time, shown in the inset of Fig. 4(b), have a nonmonotonic behavior as a function of  $R$  (similarly to what observed for  $\sigma^2$ ). The higher values of  $Nu$  are observed for the transition case  $N_y = 16$  [see inset of Fig. 4(b)] which has also the largest vertical velocity (see Fig. 3). We remark that, since in Fig. 4(b) the Nusselt numbers are plotted at fixed Rayleigh number, their dependence on  $R$  is not affected by the faster growth of the mixing layer in the 2D case, but only on the increased correlation between the vertical velocity and density fluctuations. This stronger correlation is also responsible for the larger values of density variance in the 2D simulations.

The bidimensionalization of the dynamics is clearly visible in the horizontal sections of the density field. The four sections shown in Fig. 5 are taken at the midplane  $z = 0$ , at time  $t = 3.5\tau$ , for the cases with  $N_y = 16, 24, 32, 512$ . Although we seed all the simulation with a three-dimensional initial perturbation at the interface, the systems with smaller  $L_y$  lose completely the  $y$  dependence as they evolve and then follow a 2D dynamics. Conversely, in the cases with large  $L_y$  the density field displays 3D structures and the 3D dynamics lasts for longer. In the case  $N_y = 24$ , at this time which correspond to the transition (see Fig. 3) we observe a coexistence of regions which are already 2D and others in which 3D structures still persist. These structures are squeezed in the thin layer, and therefore they assume an elongated shape in the  $x$  direction. The squeezing of the fingers causes the increase of the correlation length  $\lambda_x$ , which is observed in the cases  $N_y = 16, 24$  as shown in Fig. 4.

A quantitative measure of the bidimensionalization of the system is provided by the 2D index:

$$\chi(t) = \left\langle \frac{\langle \rho(x, y, z = 0, t) \rangle_y^2}{\langle \rho^2(x, y, z = 0, t) \rangle_y} \right\rangle_x, \quad (3)$$

which varies in the range  $[0, 1]$ . In case of 3D homogeneous dynamics, the average of the density fluctuations in the  $y$  direction at fixed  $x$  and  $z = 0$  vanishes, and therefore  $\chi = 0$ . Conversely, if the density field is independent on the  $y$  coordinate, then the averages  $\langle \rho(x, y, z = 0, t) \rangle_y^2$  and  $\langle \rho^2(x, y, z = 0, t) \rangle_y$  are equal, and hence  $\chi = 1$ . The temporal evolution of  $\chi(t)$  is shown in Fig. 6. In the cases with the smaller  $L_y$  ( $N_y = 2, 4$ ) the value of the index is  $\chi(t) = 1$  at all times, because the system does not develop 3D instabilities and the dynamics remains fully 2D. Increasing  $L_y$ , the initial value of  $\chi(t)$  decreases, signaling the presence of 3D structures in the density field in

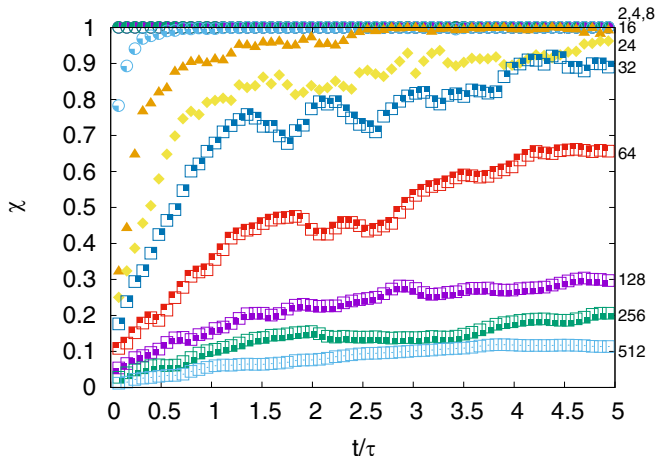


FIG. 6. Time evolution of the two-dimensional index  $\chi$  for different values of  $N_y$  (see labels). Colors and symbols are the same of Fig. 2.

the early stage of the evolution. When the horizontal scale of these structures grows and becomes larger than  $L_y$ , the system recovers the 2D dynamics and the index approaches (slowly) the 2D value  $\chi(t) = 1$ . Increasing  $L_y$ , the bidimensionalization is achieved at longer times. For the cases with larger  $L_y$  ( $N_y > 24$  in our set of simulations) the value of the index remains  $\chi(t) < 1$  for all times, indicating that the complete bidimensionalization is never achieved. We remark that we can expect  $\chi = 0$  only when the number of points  $N_y$  in the  $y$  directions is large enough to give a zero average in the numerator of (3).

## V. CONCLUSIONS

We have studied the effects of the dimensionality on mixing processes in the Darcy-Rayleigh-Taylor system by means of extensive direct numerical simulations in a periodic domain with variable horizontal width.

Our results confirm that the growth of the mixing layer is faster for thin fluid layers, in agreement with previous findings [13]. The dimensionality of the system influences also the properties of the convective structures (“fingers”) within the mixing layers. In the 2D cases, the density field inside the fingers is less mixed and it is more correlated with the vertical velocity than in 3D.

The transition from the 3D to the 2D regimes is observed when the typical width of the fingers, which is quantified in terms of the horizontal correlation scale  $\lambda_x$ , becomes larger than the confining scale  $L_y$ . Interestingly, the horizontal scale  $\lambda_x$  grows in time because of the intricate processes of merging and diffusive coarsening of fingers. Given that the process of coarsening (which follows a diffusive law) is very slow compared to the evolution of the mixing layer (which grows linearly in time), in most cases it is possible to classify the evolution of the DRT system in two classes, which follows either the ideal 2D or the 3D dynamics. Nevertheless, for the intermediate cases in which the width  $L_y$  of the layer is close to the initial width of the fingers, we observe a dimensional transition from an initial 3D regime to the 2D regime at late times, caused by the coarsening of the fingers.

In the ideal case of a domain with infinite vertical extension, the coarsening of the fingers could, in principle, continue until they reach the horizontal confining scale, even if the latter is very large. This would eventually lead to a dimensional transition for arbitrary large  $R$ . Anyway, this would require a very long time, because the coarsening is slow. In real cases, in which the domain is finite, the transition can be observed only in a narrow range of  $R$ .

If the horizontal scales are comparable ( $L_x \simeq L_y$ ), then the transition leads to a 1D regime. The 1D regime has been investigated in the turbulent RT case [31], in which a subdiffusive growth of the mixing layer  $h(t) \sim t^{2/5}$  is observed.

We note that our results have been obtained with periodic boundary conditions (BC) also in the confined direction. When the flow is confined in 2D (or quasi-2D) geometries by rigid boundaries, the dynamics is influenced by the absence of wall-normal flow and the friction with the side walls, which dissipates part of the kinetic energy. Nonetheless, in the case of turbulent flows, it has been shown that the presence of boundaries in experimental studies with thin fluid layers does not change qualitatively the results of the simulations with periodic BC (in particular the coexistence of a direct and inverse cascade). In the case of porous media, the Darcy flow is dominated by the friction with the medium everywhere, therefore the effects of the friction with side walls is expected to be very small, if any. The role of no-penetration BC on the dimensional transition is less clear. The absence of normal flow across the boundaries could hinder the development of the 3D structures in the case in which the confining direction is of the same order of the horizontal size of the fingers. This effect could shift the dimensional transition to slightly larger values of the confinement number  $R$  with respect to those observed in our simulations with periodic BC. A comparison of our results with numerical and/or experimental studies in the presence of no-normal-flow boundaries could help to clarify this issue.

- 
- [1] P. G. Saffman and G. I. Taylor, The penetration of a fluid into a porous medium or hele-shaw cell containing a more viscous liquid, *Proc. R. Soc. Lond. A* **245**, 312 (1958).
  - [2] G. Boffetta and A. Mazzino, Incompressible Rayleigh–Taylor turbulence, *Annu. Rev. Fluid Mech.* **49**, 119 (2017).
  - [3] Y. Zhou, Rayleigh–Taylor and Richtmyer–Meshkov instability induced flow, turbulence, and mixing. ii, *Phys. Rep.* **720-722**, 1 (2017).
  - [4] Herbert E. Huppert and Jerome A. Neufeld, The fluid mechanics of carbon dioxide sequestration, *Annu. Rev. Fluid Mech.* **46**, 255 (2014).
  - [5] J. Ennis-King and L. Paterson, Role of convective mixing in the long-term storage of carbon dioxide in deep saline formations, *SPE J.* **10**, 349 (2005).
  - [6] P. A. Tsai, K. Riesing, and H. A. Stone, Density-driven convection enhanced by an inclined boundary: Implications for geological co<sub>2</sub> storage, *Phys. Rev. E* **87**, 011003 (2013).
  - [7] H. Emami-Meybodi, H. Hassanzadeh, C. P. Green, and J. Ennis-King, Convective dissolution of co<sub>2</sub> in saline aquifers: Progress in modeling and experiments, *Int. J. Greenhouse Gas Contr.* **40**, 238 (2015).
  - [8] P. M. J. Trevelyan, C. Almarcha, and A. De Wit, Buoyancy-driven instabilities of miscible two-layer stratifications in porous media and hele-shaw cells, *J. Fluid Mech.* **670**, 38 (2011).
  - [9] S. S. Gopalakrishnan, J. Carballido-Landeira, A. De Wit, and B. Knaepen, Relative role of convective and diffusive mixing in the miscible Rayleigh–Taylor instability in porous media, *Phys. Rev. Fluids* **2**, 012501 (2017).
  - [10] M. De Paoli, F. Zonta, and A. Soldati, Rayleigh–Taylor convective dissolution in confined porous media, *Phys. Rev. Fluids* **4**, 023502 (2019).
  - [11] R. Arun, S. T. M. Dawson, P. J. Schmid, A. Laskari, and B. J. McKeon, Control of instability by injection rate oscillations in a radial hele-shaw cell, *Phys. Rev. Fluids* **5**, 123902 (2020).
  - [12] Y. Nakanishi, A. Hyodo, L. Wang, and T. Suekane, Experimental study of 3d Rayleigh–Taylor convection between miscible fluids in a porous medium, *Adv. Water Res.* **97**, 224 (2016).
  - [13] G. Boffetta, M. Borgnino, and S. Musacchio, Scaling of Rayleigh–Taylor mixing in porous media, *Phys. Rev. Fluids* **5**, 062501 (2020).
  - [14] A. Alexakis and L. Biferale, Cascades and transitions in turbulent flows, *Phys. Rep.* **767-769**, 1 (2018).
  - [15] A. Celani, S. Musacchio, and D. Vincenzi, Turbulence in More Than Two and Less Than Three Dimensions, *Phys. Rev. Lett.* **104**, 184506 (2010).

- [16] S. J. Benavides and A. Alexakis, Critical transitions in thin layer turbulence, *J. Fluid Mech.* **822**, 364 (2017).
- [17] S. Musacchio and G. Boffetta, Split energy cascade in turbulent thin fluid layers, *Phys. Fluids* **29**, 111106 (2017).
- [18] G. Boffetta, F. De Lillo, and S. Musacchio, Bolgiano scale in confined Rayleigh–Taylor turbulence, *J. Fluid Mech.* **690**, 426 (2012).
- [19] G. Boffetta, A. Mazzino, S. Musacchio, and L. Vozella, Kolmogorov scaling and intermittency in Rayleigh–Taylor turbulence, *Phys. Rev. E* **79**, 065301 (2009).
- [20] M. Chertkov, Phenomenology of Rayleigh–Taylor Turbulence, *Phys. Rev. Lett.* **91**, 115001 (2003).
- [21] A. Celani, A. Mazzino, and L. Vozella, Rayleigh–Taylor Turbulence in Two Dimensions, *Phys. Rev. Lett.* **96**, 134504 (2006).
- [22] M. Muskat, *The Flow of Homogeneous Fluids through Porous Media* (McGraw–Hill, New York, 1937).
- [23] D. A. Nield and A. Bejan, *Convection in Porous Media* (Springer, Berlin, 2006).
- [24] W. P. Breugem, B. J. Boersma, and R. E. Uittenbogaard, The influence of wall permeability on turbulent channel flow, *J. Fluid Mech.* **562**, 35 (2006).
- [25] R. A. Wooding, The stability of an interface between miscible fluids in a porous medium, *J. Appl. Math. Phys.* **13**, 255 (1962).
- [26] J. P. Heller, Onset of instability patterns between miscible fluids in porous media, *J. Appl. Phys.* **37**, 1566 (1966).
- [27] W. H. Cabot and A. W. Cook, Reynolds number effects on Rayleigh–Taylor instability with possible implications for type Ia supernovae, *Nat. Phys.* **2**, 562 (2006).
- [28] S. B. Dalziel, P. F. Linden, and D. L. Youngs, Self-similarity and internal structure of turbulence induced by Rayleigh–Taylor instability, *J. Fluid Mech.* **399**, 1 (1999).
- [29] G. Boffetta, F. De Lillo, and S. Musacchio, Nonlinear Diffusion Model for Rayleigh–Taylor Mixing, *Phys. Rev. Lett.* **104**, 034505 (2010).
- [30] G. Sardina, L. Brandt, G. Boffetta, and A. Mazzino, Buoyancy-Driven Flow Through a Bed of Solid Particles Produces a New Form of Rayleigh–Taylor Turbulence, *Phys. Rev. Lett.* **121**, 224501 (2018).
- [31] G. Boffetta, F. De Lillo, and S. Musacchio, Anomalous diffusion in confined turbulent convection, *Phys. Rev. E* **85**, 066322 (2012).